Kovove Mater. 63 2025 251–262
DOI: 10.31577/km.2025.4.251

Study of mechanical and microstructural properties of arc-produced aluminum 6061 alloy thin plate and block using additive manufacturing

Nalini Lekkala[1,2]*, Kondapalli Siva Prasad[3], Chalamalasetti Srinivasa Rao[4]

[1] *AU Trans-Disciplinary Research Hub, Department of Mechanical Engineering, Andhra University, Visakhapatnam, Andhra Pradesh-530003, India*
[2] *Department of Mechanical Engineering, Vignan's Institute of Information Technology, Duvvada, Visakhapatnam, Andhra Pradesh-530049, India*
[3] *Department of Mechanical Engineering, Anil Neerukonda Institute of Technology and Sciences, Sangivalasa, Visakhapatnam, Andhra Pradesh-531162, India*
[4] *Department of Mechanical Engineering, AU College of Engineering Andhra University, Andhra University, Visakhapatnam, Andhra Pradesh-530003, India*

Received 2 June 2025, received in revised form 7 November 2025, accepted 10 November 2025

Abstract

Directed Energy Deposition (DED-Arc), an advanced additive manufacturing process that utilizes an arc heat source, is commonly employed to fabricate large-scale metal components with complex geometries. The technique involves applying layers of metal, typically in wire or powder form, and melting it using an electric arc. This research investigates the microstructural and mechanical characteristics of DED-Arc, employing GMAW (Gas Metal Arc Welding) of the plate and block components of Aluminum 6061 alloy. Microscopic analyses are performed using Optical Microscopy, Scanning Electron Microscopy (SEM), X-ray diffraction (XRD), and Energy Dispersive X-ray spectroscopy (EDX). Fine-structure analysis revealed that the grain structure consists of distinct interlayer and intralayer regions along the vertical direction of both the plate and block. In contrast, the horizontal direction exhibits a relatively homogeneous microstructure. Additionally, similar inter-layer and intra-layer features are observed along the crosswise dimension in the block. Pores of both macro and micro sizes were detected in the samples of the plate and block. Moreover, the microvoids observed within the block samples were likely caused by inadequate penetration between adjacent layers. Second-phase particles, including α-Al and β-phase Mg_2Si, were found embedded in the matrix and concentrated near the edges. Secondary phase particles were identified both within the matrix and near the boundaries. Microhardness and tensile tests are used to examine the material's mechanical properties. It was observed that the typical value of hardness increases from the lower to the upper area across the plate and block. The 6061 Al alloy plate produced by DED-Arc demonstrates better tensile properties compared to the cast 6061 Al alloy. Due to the presence of significantly larger microvoids and pores in block samples, their tensile properties were considerably reduced. All specimens extracted from the block and thin plate exhibited ductile fractures.

Key words: Aluminum 6061, direct energy deposition, arc energy source, mechanical properties, thin plate, block, microstructure

1. Introduction

The effective rapid prototyping approach for creating near-net form large-scale components is additive manufacturing [1]. DED-Arc utilizes wire as a feedstock with an arc of electricity as the heat input. Large components can be fabricated using this technique, which is considered one of the most effective meth-

*Corresponding author: e-mail addresses: lekkalanalini0426@gmail.com , nalini.mech@vignaniit.edu.in

ods, such as additive manufacturing [2]. Various welding techniques have been employed during the metal fabrication process [3–5]. The GMAW constitutes a prominent additive manufacturing and welding process that creates an arc of electricity across a substrate. The wire is usually positioned in a direction during deposition that is perpendicular to the surface. A uniform and smooth welding bead primarily depends on the orientation of the wire feed [6]. Fronius developed the technology Cold Metal Transfer (CMT), a more sophisticated MIG welding procedure designed to enhance heat input control and energy density in GMAW (Gas Metal Arc Welding) [7]. The fundamental principles within the CMT process have been explored through a comparison with the conventional MIG welding process [8]. Researchers, engineers, and designers are investing in aluminum alloys as potential structural materials for the automotive and aerospace sectors, as cited by Gerhard (2014). Due to their exceptional castability and reduced vulnerability to hot cracking, the 4xxx, 5xxx, and 2xxx series of aluminum alloys are currently the most commonly used in DED--Arc. On the other hand, because of their increased susceptibility to thermal cracking, the alloys in the 6xxx and 7xxx series present difficulties in DED-Arc [9].

The benefits of the 6xxx series include corrosion resistance, good formability, weldability, medium strength, and a lower cost compared to other aluminum alloys. This series of aluminum alloys has been the subject of numerous studies [10]. Cong et al. [11] described the existence of porosity defects that may limit the usage of DED-Arc for aluminum alloys. Porosity in aluminum alloy welds is commonly attributed to hydrogen, and this is probably also true for DED-Arc metals. The solubility rate of hydrogen in liquid aluminum is 0.65 milliliters per 100 grams, whereas in solid aluminum, it is 0.034 milliliters per 100 grams [12]. According to Dinovitzer et al. [13], the wire feeding operation is significant due to leftover stresses and distortion from the AM process. The mechanical characteristics of an Al-Cu-Mg component produced using filler metals and the double-wire-arc additive technique, specifically aluminum-magnesium ER5087 and aluminum-copper ER2319, were investigated by Qi et al. [14]. Increasing the Cu/Mg ratio raised the yielding strength (YS) from 156 to 187 MPa, indicating improved mechanical characteristics; the maximum tensile strength (UTS) was 280 $\pm$ 5 MPa. Increasing Mg_2Si concentration enhances the strength of 6XXX aluminum alloys. Nevertheless, it has been demonstrated that excessive silicon in the aluminum alloy of the 6X51 type leads to decreased corrosion resistance and fracture toughness [15]. Modifying the wire speed with the aid of a passive vision system improved dimensional accuracy and investigated the weld bead width in multi-layer deposition [16]. To study the impact of GMAW processing settings on the physical dimensions of the accumulated layer, Zhao et al. [17] employed GMAW using 5356 aluminum and observed that when the scanning speed increases, the deposited layer's size reduces, and it rises linearly with arc current. To examine the differences between non-pulsed and pulsed arcs in GMAW-based DED-Arc, Luo et al. [18] used aluminum wire ER4303. Their results show that a high droplet transfer frequency may be maintained while reducing droplet size using the pulsed arc approach. According to reports, specific challenges are associated with welding aluminum alloys. Aluminum requires about the same amount of heat energy as is required to weld steel, although it has a much lower melting point (630–660 ℃) due to its extremely high thermal conductivity and fusion temperature. The dimensions of the deposited material are significantly influenced by factors such as laser power, travel speed, and wire feed rate. The GMAW-based DED-Arc method produces a non-uniform weld bead shape, especially at the beginning and conclusion of the pass. This can result in inconsistent bead geometry, poor surface polish, and decreased part accuracy [19]. Zhang et al. [20] addressed uneven surfaces caused by arc start and end by adjusting welding parameters to manage bead geometry. Several studies have utilized regression analysis to identify the relation between bead geometry and its characteristics [21]. Welding heat produces material contraction during solidification, resulting in residual stress along the bead [22]. Mughal et al. [23] created a thermo-mechanical system for predicting residual stress-related deformations. Qiu et al. investigated the microstructure and tensile properties of Ti-6Al-4V fabricated using Selective Laser Melting (SLM) followed by Hot Isostatic Pressing (HIP). The samples manufactured in the horizontal orientation exhibited higher porosity compared to those produced in the vertical orientation [24]. Mertens et al. compared the mechanical properties of Ti-6Al-4V alloy and 316L stainless steel, both fabricated using Selective Laser Melting (SLM) under similar processing conditions. The Ti-6Al-4V alloy exhibited more complex mechanical anisotropy than the stainless steel. This increased sensitivity is attributed to the lower thermal conductivity of titanium, which leads to higher residual stresses during the manufacturing process [25]. Khorasani et al. [26] investigated the impact of SLM process parameters and heat treatment on the hardness of Ti-6Al-4V components. Hardness variations were linked to melt pool rheology, porosity, and energy input. Optimal laser power and scan strategies enhanced hardness, while deviations in hatch spacing reduced it. Future work will focus on shrinkage, dimensional accuracy, and thermal behavior during processing [26]. Yang Zhao et al. utilized CMT-WAAM to fabricate 316L stainless steel plates with varying printing paths

Table 1. Composition of Al 6061 (%)

Element	Mn	Zn	Cu	Fe	Ti	Cr	Mg	Si	Al
(Al 6061) wire	0.025	0.032	0.18	0.35	0.013	0.098	0.98	0.49	97.39

Table 2. Measurement results of the response for the experimental plan

Sample No.	V_w (m min^{-1})	W_{fs} (m min^{-1})	V (V)	Width (mm)
1	0.3	4	12	2.68
2	0.3	6	14	4.09
3	0.3	8	16	6.40
4	0.6	4	14	2.79
5	0.6	6	16	4.13
6	0.6	8	12	3.53
7	0.9	4	16	2.51
8	0.9	6	12	2.39
9	0.9	8	14	4.24

and evaluated their tensile properties in three orientations. Strength met standards, but fracture strain was slightly lower. HL-T4 showed the highest strength and the lowest ductility, while VL-T4 had the lowest strength and the highest fracture strain. Metallography showed austenitic grains, where finer grains improved strength but reduced ductility, except in VL-T4 due to uniform grain orientation [27].

Aluminum 6061 exhibits excellent mechanical properties, including high strength, corrosion resistance, and weldability, which make it widely used in various industrial applications, as reported in the literature. It is commonly employed in industries including aerospace, automotive, and marine, as well as for structural applications. Although Aluminum 6061 is widely used in traditional manufacturing, there has been limited research on its potential applications in additive manufacturing. The novelty of the present work lies in employing the GMAW-based DED-Arc process to fabricate two distinct geometries – a thin plate and a block – and performing a systematic comparison of their metallurgical and mechanical behavior. Unlike earlier reports, this study not only demonstrates the feasibility of producing Al 6061 components with this method but also provides new insights into how geometry influences defect formation, microstructural evolution, and property variation.

2. Materials and methods

2.1. Materials

The GMAW-based DED-Arc method was employed to fabricate both a thin plate and a block. The Al 6061 alloy plate, with a width of 49 mm, a length of 145 mm, and a thickness of 19 mm, serves as the substrate. The material for deposition is provided in the form of a spool containing an aluminum alloy wire measuring 1.2 mm in diameter. Before initiating the production process, the substrate surface should be carefully rinsed with acetone and leveled to ensure proper flatness. The chemical composition of the deposited wire is presented in Table 1.

2.2. DED-Arc configuration

A block and a thin plate were fabricated using Al 6061 alloy in the form of wire to investigate their mechanical and microstructural characteristics utilizing CMT-MIG welding equipment. KR8R1620 system equipped with an integrated Fronius CMT setup, integrated with a wire feeding configuration, an inert gas atmosphere, and an enhanced power supply. Pure argon (Ar) shielding gas isolates molten weld pools, preventing contamination from atmospheric gases. Before fabrication, the substrate surface should be cleaned with acetone to eliminate oils and grease, ensuring a flawless welding process. To prevent the substrate plate from buckling due to temperature changes during the deposition process, clamps were used to secure it to the workbench. Figure 1 displays a schematic representation of the entire system.

2.3. Parameters during fabrication

The L9 orthogonal Taguchi array optimization method was employed to determine the optimal parameters for electric potential, filler wire speed, and welding speed. Nine trials were conducted, resulting in nine weld beads. The best weld bead was identified through *ANOVA* analysis, and the corresponding parameters were utilized for the deposition of the plate and block [28]. Table 2 presents the measurement re-

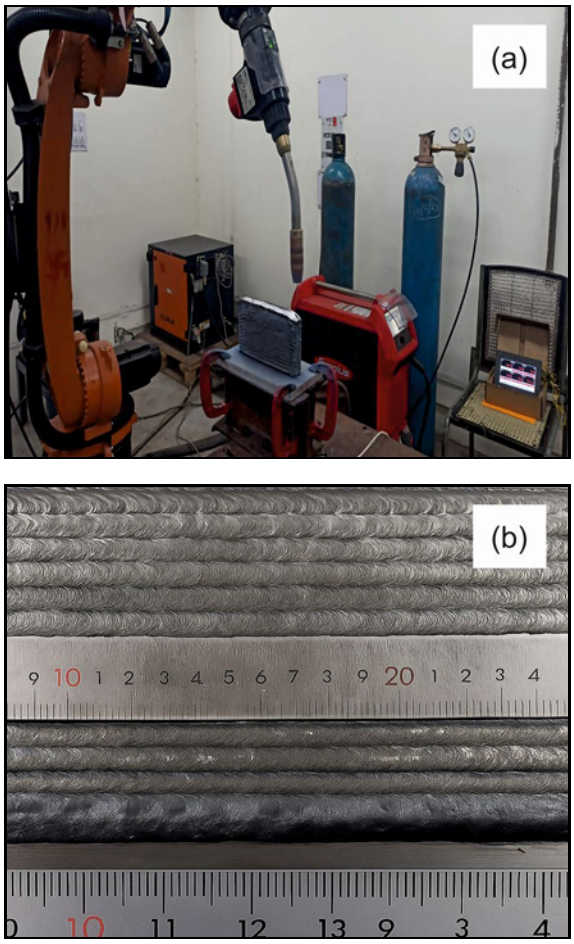

Fig. 1. (a) Fabrication of the block and (b) fabrication of the thin plate.

sults obtained from the experimental plan. The parameters considered for the study include the wire feed rate (V_w), feed speed (V_{fs}), and applied voltage (V). The corresponding responses in terms of the measured cut width are listed for each experimental run. The data were used to analyze the influence of these process variables on the resulting width and to identify the optimal combination of parameters for achieving the desired machining accuracy. Thin plate and block were produced by applying specific processing conditions determined from the most effective weld bead trial optimization. The production of the thin plate and block involved controlled operating conditions, with a welding speed set at 0.6 m min^{-1}, a filler wire speed of 8 m min^{-1}, and an electric potential of 16 V applied throughout the process. An interval time of 85 seconds was consistently maintained in the middle of each layer throughout the manufacturing process. The z-axis was raised by 1.2 mm for each layer, ensuring the filler wire tip remained positioned 1.3 mm above the substrate. The angle between the substrate plate and the torch nozzle was consistently maintained at

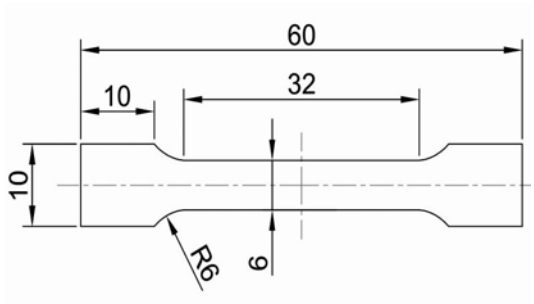

Fig. 2. Tensile sample dimensions.

89° , while the feed wire tip was kept 18 mm away from the nozzle. The deposition process was conducted in a simultaneous mode, with successive layers deposited in alternating directions.

2.4. Material characterization tests

At the outset, the dimensions of the as-fabricated thin plate were measured to be 110 × 120 × 2 mm^3, and the fabricated block measured approximately 200 × 47 × 90 mm^3. The microstructural investigation was carried out using an optical microscope, EDX analysis, SEM, and XRD. Square samples measuring 13 mm in length were obtained through wire-cut electrical discharge machining (EDM) from the upper, central, and lower sections of the thin plate. To accomplish the intended objective of a submicron-level surface finish, the metallographic examinations were commenced by polishing with emery paper and followed by diamond polishing. The surface was etched for 10 seconds using a mixture of 25 milliliters each of HCl, HNO_3, and CH_3OH, along with 1–2 drops of hydrogen fluoride. Following metallographic sample preparation, microstructural images were obtained using an optical microscope. The micro-area composition was analyzed using Scanning Electron Microscopy (SEM) coupled with Energy-Dispersive X-ray Spectroscopy (EDX). The development of the secondary phase was revealed by XRD analysis.

2.5. Mechanical property tests

In compliance with the ASTM E8M standard, a total of five tensile samples (Fig. 2) were prepared, three of which were obtained in the direction of vertical build-up, while two were acquired from thin plates in the direction of horizontal welding. A set of three tensile samples was extracted along the weld line from the upper, central, and lower parts of the block. A tensile test performed on a SANS 5504 tensile testing machine was used to measure elongation, yield strength, and ultimate tensile strength. Samples of 15 mm in length were taken from the broken tensile specimens

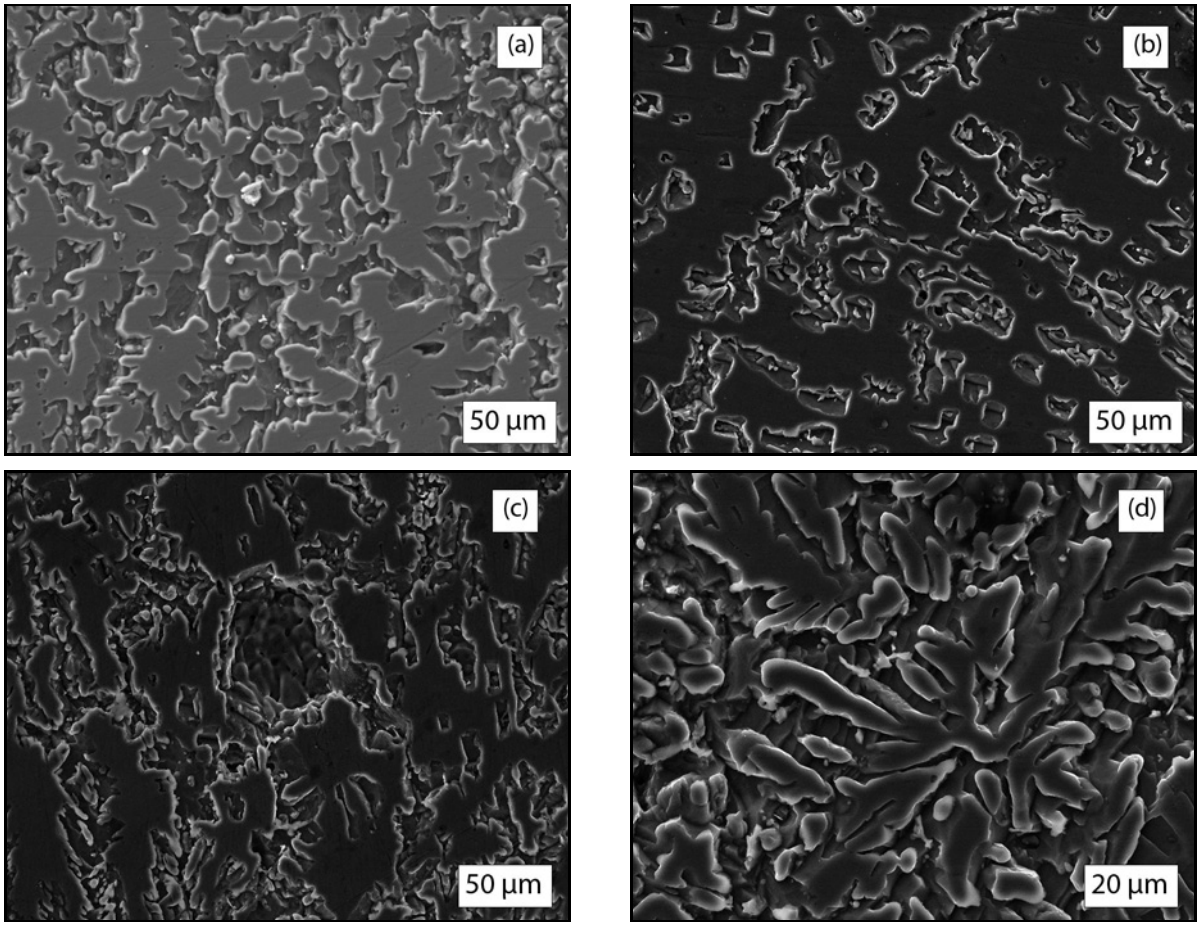

Fig. 3. (a) Base plate, (b) microporosity of thin plate, (c) coarse grains of block, and (d) isometric grain for thin plate.

to characterize the fracture surface morphology using SEM. To evaluate the microhardness of the plate and block, 10 mm diameter specimens are considered from the bottom, center, and top areas of the thin plate. The microhardness testing was carried out utilizing the (HVS 1000B) Vickers hardness tester. Figure 3 displays the measurements of tensile samples taken from a thin plate and a block fabricated through arc-based manufacturing.

3. Results and discussion

3.1. Microstructural characterization

For the thin plate sample, the dilution zone between the substrate plate and the weld bead is clear, as shown in Fig. 3a. The microstructural analysis demonstrates a gradient in particle size, where fine particles dominate the upper region of the plate, while relatively coarser particles are observed toward the bottom, as seen in Fig. 3d. The thin plate is characterized by a high density of micropores, which primarily arise due to hydrogen entrapment in the molten pool during solidification. However, the number of microcracks in this sample is comparatively low. Furthermore, macropores are rarely detected, indicating that although porosity is present, it is limited mostly to small-sized pores. The relatively finer and more uniform microstructure of the thin plate suggests superior metallurgical quality when compared with the block sample. Van Thao Le et al. [28] investigated the impact of heat on walls fabricated through DED-Arc and found that reducing the amount of thermal energy applied improves both the metallurgical and mechanical properties [29]. In contrast, the block sample exhibits more pronounced defects, both in terms of porosity and microstructural irregularities. Air gaps are commonly observed between successive layers, particularly in regions where the layers fail to overlap properly, as shown in Fig. 3b. Figure 3c further highlights the presence of both micro- and macropores, with the block sample containing a significantly higher pore density compared to the thin plate. Cracks are frequently identified along the interlayer boundaries, and these defects can be attributed to the repeated reheating of previously deposited layers during the fabrication of multilayers. The microstructure of the block, illustrated in Fig. 3d, consists predominantly of sparsely distributed and nonuniform columnar grains, accom-

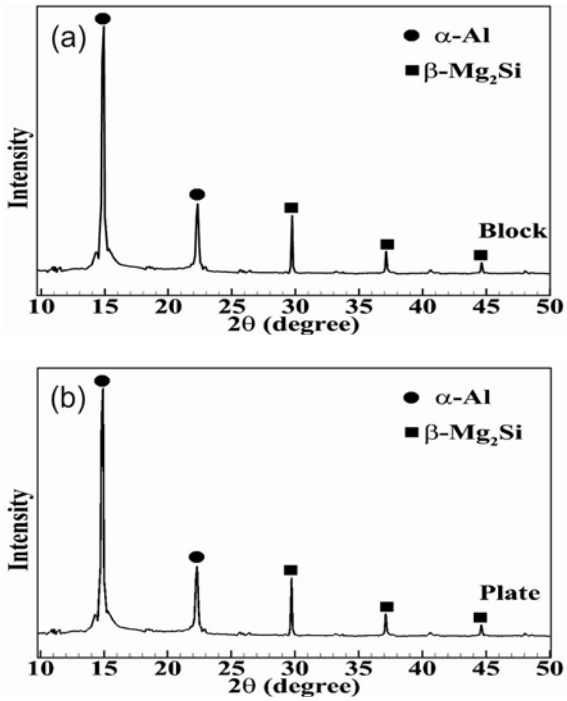

Fig. 4. XRD results of plate and block of 6061 Al alloy.

panied by equiaxed grains in certain regions. Overall, the grains in the block appear coarser than those in the thin plate. The excessive porosity in the block is likely caused by surplus hydrogen in the weld pool, while the shielding gas flow rate and volumetric flow rate of deposition also play significant roles. At higher gas flow rates, convective cooling accelerates the solidification of the melt pool, restricting the escape of trapped gases, thereby increasing porosity. Conversely, lower gas flow rates extend the molten state, enabling gases to escape more effectively.

From this comparative analysis, it is evident that the thin plate exhibits a finer microstructure with fewer defects, whereas the block sample is more prone to porosity, air gaps, and cracking, ultimately leading to inferior metallurgical and mechanical properties.

Figure 4 depicts XRD analysis of block samples and a thin plate of 6061 Al alloy deposited through DED-Arc. The XRD analysis reveals the phases present in the samples, which are composed of α-Al and the β-phase of Mg_2Si. Diffraction peaks for block samples and thin plates show the positions of α-Al and β-phase Mg_2Si. The block sample exhibits a higher peak intensity of Mg_2Si compared to the thin plate sample, indicating a greater development of the Mg_2Si phase. SEM provides detailed insights into the internal characteristics of both block and thin plate samples.

Figure 5 presents the SEM micrographs and EDX compositional analysis of both the block and thin plate samples, providing insight into their microstructural and chemical characteristics. Figure 5d highlights an equiaxed dendrite observed at the layer interface of the block sample, indicating a relatively uniform grain structure within the deposited layers. This feature reflects the solidification behavior and thermal gradients present during the DED-Arc process for the block sample. Figures 5e,f show the EDX analysis results for the thin plate and block samples, respectively, revealing the elemental composition and distribution across the deposited material. The EDX maps confirm the presence of the expected alloying elements and demonstrate minimal segregation between layers.

Comparing the thin plate and block samples, it is evident that the thin plate exhibits a more refined microstructure, consistent with reduced heat input and faster cooling rates. These observations support the conclusion that thermal management during deposition strongly influences the resulting microstructure. Overall, Fig. 5 provides a comprehensive view of both structural morphology and chemical uniformity, serving as a basis for understanding the differences in mechanical and metallurgical properties.

3.2. Microhardness

Microhardness tests were conducted on the middle, bottom, and top areas of the fabricated plate and block. Figure 6a illustrates the process of determining microhardness values on both sides of the thin plate's centerline, at intervals of 6, 16, and 26 mm. As shown in Fig. 6b, microhardness values were recorded at the center and edges of the block, at distances of 11, 21, and 32 mm from the centerline. The microhardness levels of both components vary across different locations. The microhardness values of both components exhibit noticeable variation across various locations. This inconsistency indicates non-uniform material properties throughout the samples. Due to differences in microstructure and shape, the microhardness values of both the block and thin plate increase gradually, ranging from the base to the exterior. Both the block and thin plate show reduced microhardness at their lower sections, while the middle regions show moderate values, and the top regions display high microhardness values. The microhardness values in the block are higher along the edges than at the center, as the edge region has a finer grain structure as opposed to the coarser grain structure in the middle. The lowest microhardness value of 56.2 HV was noted at the middle-bottom area of the block. In contrast, the bottom region of the thin plate exhibited a slightly higher microhardness of 58.4 HV. The top region of the thin plate recorded the highest microhardness at 102.3 HV, followed by the top portion of the block, which reached 93.6 HV. Additionally, the middle region of the thin plate measured a hardness of 74.5 HV, while the bottom region of the block registered 78.9 HV.

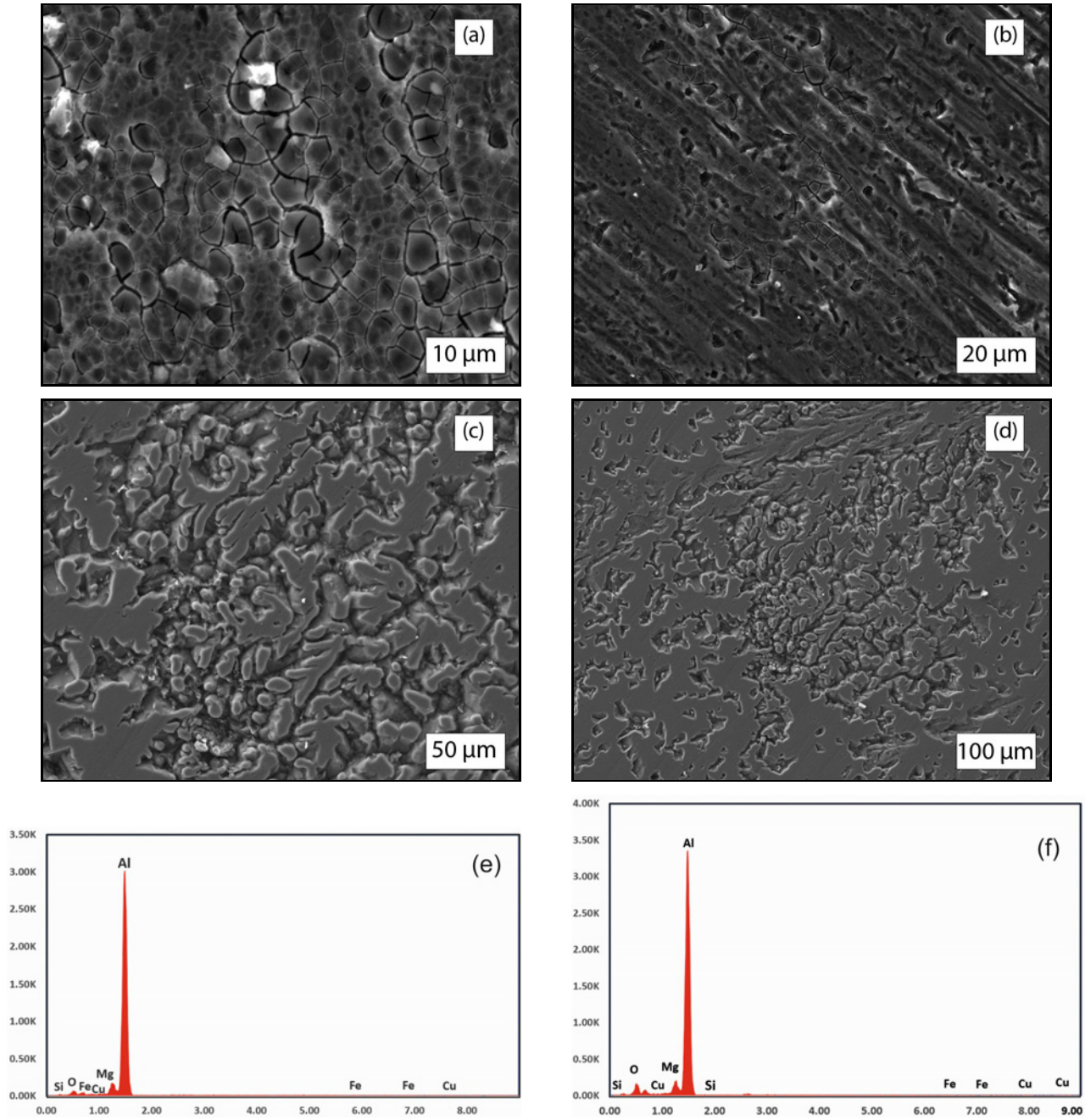

Fig. 5. SEM and EDX analysis of the block and thin plate specimens are presented as follows: (a) and (b) show the plate SEM images, (c) and (d) illustrate block SEM images, (e) and (f) display the results of the EDX for the block and plate.

3.3. Tensile characteristics

Figure 2 shows the schematic representation of the tensile test specimen used in the present study. The specimen has an overall length of 60 mm, a gauge length of 32 mm, and a width of 6 mm in the reduced section. The end sections are 10 mm wide to facilitate proper gripping during testing. A fillet radius of 6 mm is provided between the grip and gauge sections to minimize stress concentration. This geometry conforms to the standard miniature tensile specimen dimensions commonly used for material characterization.

The block and thin plate underwent tensile testing made from 6061 aluminum alloy to assess their mechanical properties. From the thin plate, two specimens oriented vertically were extracted at the center, and two specimens oriented horizontally were gathered from the top and bottom areas. Three samples oriented horizontally were collected from the lower, middle, and upper regions of the block. Figure 7 shows the acquired properties of tensile, including yield, elon-

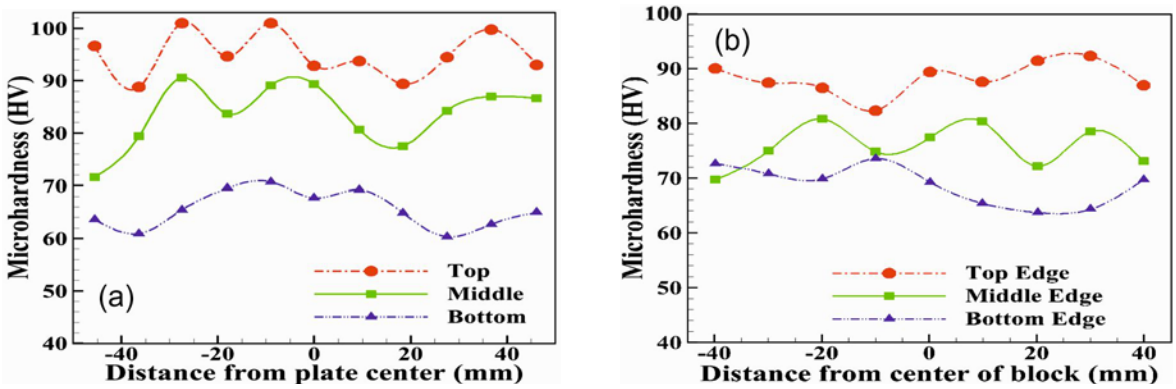

Fig. 6. Microhardness results of the plate and block of 6061 Al alloy.

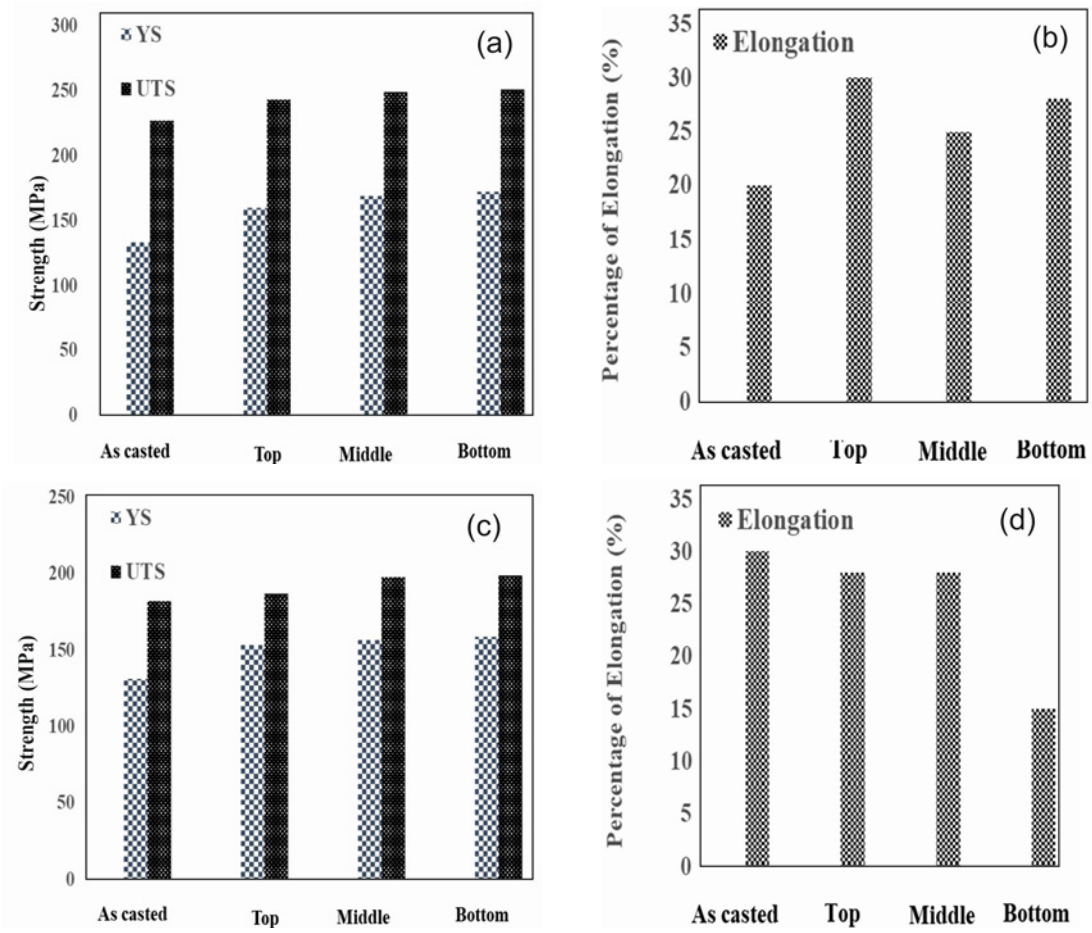

Fig. 7. Tensile mechanical performance of plate and block specimens.

gation (EL) and ultimate tensile strength (UTS) are key structural properties with UTS representing the maximum stress the material can withstand, YS refers to the yield strength, which is the stress level where the material starts to undergo irreversible deformation and EL represents the material's capacity to undergo elongation prior to fracture. The filler wire for the 6061 aluminum alloy exhibits a UTS of 256 MPa, a YS of 126 MPa, and an elongation capacity of 25 %. The aluminum alloy's ultimate strength and yield stress in its as-cast condition are 216.5 and 87.2 MPa, respectively. An elongation of 23.5 % is observed [30]. The mean tensile characteristics of thin plate samples are as follows: 29.4 % for EL, 242.5 MPa for UTS, and 158.4 MPa for YS. The average UTS, YS, and EL values for block samples are 150 MPa, 191.6 MPa, and 17.8 %, respectively. The block sample yielded a UTS of 63 MPa, a YS of 27 MPa, and an elongation of 5 %.

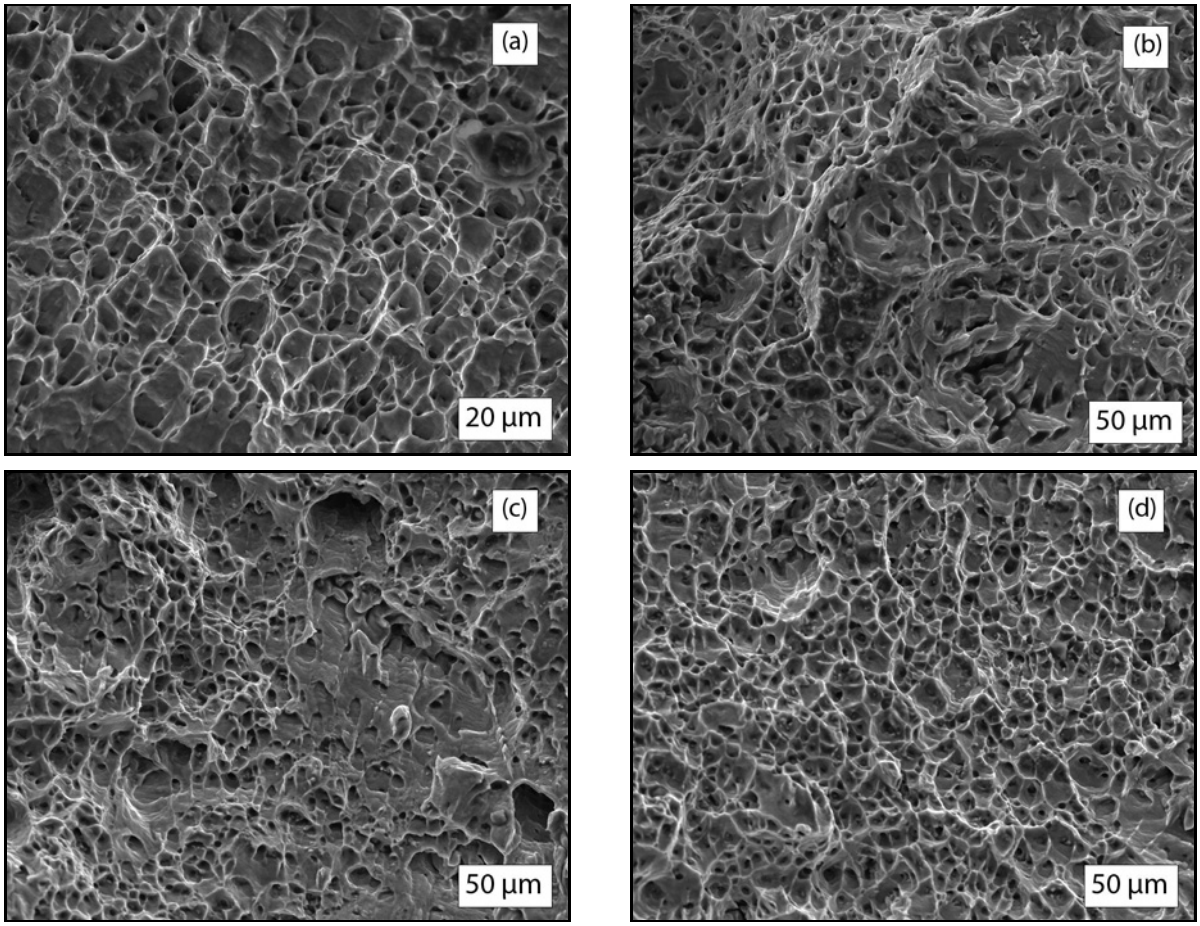

Fig. 8. SEM pictures of fractured zones in arc-fabricated Al6061 alloy: (a) and (b) depict plate samples, (c) and (d) depict block samples.

Meanwhile, the thin plate demonstrated a lower tensile strength of 13 MPa, a higher yield strength of 35 MPa, and an identical elongation of 5 %.

Block samples exhibited lower tensile characteristics due to greater air gaps and porosity between parallel layers, as seen in Fig. 7c, whereas arc-manufactured 6061 Al alloy thin plates had greater tensile values than as-casted samples, Fig. 7a.

The impact of porosity on mechanical characteristics was primarily affected by the size, quantity, and distribution of pores. It can create stress concentration, which can significantly affect the material strength. The porosity can significantly impair ductility by creating localized weaknesses within the material, which can limit its ability to deform plastically under stress. Increasing porosity diminishes material ductility and raises the risk of brittle fracture. The horizontal YS and UTS of thin plate samples range from 155 to 185 MPa and 235 to 265 MPa, respectively, with an EL varying between 32 and 34 %. The yield strength of the thin plate samples in the vertical direction varies between 152 and 157 MPa, while their ultimate tensile strength spans from 223 to 256 MPa, with elongation varying between 28 and 32 %. Tensile characteristics are weaker in the transverse direction than in the horizontal direction due to the inhomogeneous microstructure at fusion zones between layers. Figure 8 presents SEM images of fractured regions in block and thin plate samples of 6061 Al alloy that were fabricated. Particles of the finer secondary phase were implanted in the center of dimples on the surface, visible in both block and thin plate samples. The surface of the cracked region contains pores and second-phase cracks. Figure 8c shows that the block samples exhibit fewer quasi-cleavage planes and a higher number of pores, leading to reduced plasticity and load-carrying capacity. Table 3 summarizes the mechanical properties of Al 6061 alloy fabricated using different additive manufacturing techniques and the conventional 6061-T6 process. Variations in hardness, tensile strength, yield strength, and elongation are evident across WAAM, SLM, and LPBF due to differences in heat input and cooling rates. The LPBF process exhibits superior strength and hardness due to its refined microstructure, whereas SLM shows reduced values due to porosity and residual stresses. WAAM offers moderate mechanical performance influenced by thermal cycling and grain coarsening. Overall, con-

Table 3. Summary of the mechanical properties of Al 6061 alloy reported in previous studies using WAAM and other additive manufacturing processes

Properties	WAAM	SLM	LPBF	6061-T6 conventional
Hardness	89	54	130	95
Ultimate Tensile Strength	280	130	268	310
Yield Strength	220	60	240	276
Elongation	12	15	26	12

Table 4. Mechanical properties of the Al 6061 thin plate and block fabricated in the present study

Sample	YS (MPa)	UTS (MPa)	Elongation (%)	Microhardness, HV
Thin plate	150.0	242.5	29.4	102.3 (top)/74.5 (mid)/58.4 (bottom)
Block	158.4	191.6	17.8	93.6 (top)/56.2 (mid)/78.9 (bottom)
Bulk 6061-T6 (Literature)	155	205	25.5	99 (top)/71.2 (mid)/68.8 (bottom)

ventional 6061-T6 demonstrates the highest strength, reflecting the benefits of controlled heat treatment.

4. Conclusions

Using the GMAW-based DED-Arc technique, a thin plate measuring $110 \times 120 \times 2\,\mathrm{mm}^3$ and a block measuring $200 \times 47 \times 90\,\mathrm{mm}^3$ were produced from 6061 aluminum alloy wire. The upcoming sections provide an in-depth analysis of the mechanical characteristics and microstructure of the block and thin plate specimens. Table 4 presents the mechanical properties of Al 6061 thin plate and block fabricated in the present study and compares them with the reported values of bulk 6061-T6 alloy. The thin plate exhibits higher ultimate tensile strength and elongation, indicating better ductility and a more balanced strength compared to the block. The block shows relatively higher yield strength but reduced elongation, attributed to its coarser grain structure and heat accumulation during deposition. Microhardness measurements reveal non-uniformity across the top, mid, and bottom regions due to varying thermal gradients during solidification. Overall, the mechanical performance of the fabricated samples is comparable to the conventional 6061-T6 alloy, demonstrating the effectiveness of the adopted processing route.

– DED-Arc process results in 6061 Al alloy thin plates and blocks with a microstructure characterized by layered features and a periodic distribution along the build direction.

– Coarse-grain structures were observed in the interlayers, while fine-grain structures were found in the inner layers along the build direction. This variation was mainly due to differences in cooling rates, as well as temperature fluctuations surrounding the molten pool.

– Interstitial layers and other regions within the layers were found to contain β-phase precipitates. The quantity of heat applied to the material (which affects the variations of the rate of cooling) was the primary factor influencing the emergence of secondary particles. Silicon in 6061 aluminum alloy contributes to the formation of Mg_2Si secondary particles.

– The mean tensile characteristics for the block and plate were as follows: the YS was 158.4 MPa and 150 MPa, respectively, while the UTS are 242.5 MPa for the thin plate and 191.6 MPa for the block. The elongation values are 29.4 % for the plate and 17.8 % for the block. When compared to the 6061 Al alloy plate produced via DED-Arc, the as-cast alloy demonstrates superior tensile properties. However, while the block sample exhibits respectable yield strength, it falls short in terms of EL and UTS.

– The microhardness measurements for the thin plate revealed values of 102.3 HV at the top, 74.5 HV in the middle, and 58.4 HV at the bottom. For the block, the microhardness was recorded as 93.6 HV at the top edge, 56.2 HV at the middle edge, and 78.9 HV at the bottom edge.

– The fracture samples of both plate and block exhibit a dimple fracture mode, characteristic of ductile behavior.

Acknowledgements

The authors sincerely acknowledge the Director, CSIR-National Metallurgical Laboratory (NML), Jamshedpur, for providing the necessary facilities and support to carry out this research work.

The authors gratefully acknowledge the Advanced Research Center (ARC-AMMPC), VFSTR, Guntur, Andhra Pradesh, India, for providing the research facilities and support.

References

[1] B. Baufeld, E. Brandl, O. Biest, Wire based additive layer manufacturing: Comparison of microstructure and mechanical properties of Ti-6Al-4V components fabricated by laser-beam deposition and shaped metal deposition, Journal of Materials Processing Technology 211 (2011) 1146–1158. https://doi.org/10.1016/j.jmatprotec.2011.01.018

[2] S. W. Williams, F. Martina, A. C. Addison, J. Ding, G. Pardal, P. Colegrove, Wire + arc additive manufacturing, Materials Science and Technology 32 (2016) 641–647. https://doi.org/10.1179/1743284715Y.0000000073

[3] J. Xiong, Y. Lei, H. Chen, G. Zhang, Fabrication of inclined thin-walled parts in multi-layer single-pass GMAW-based additive manufacturing with flat position deposition, Journal of Materials Processing Technology 240 (2017) 397–403. https://doi.org/10.1007/s12206-021-0516-1

[4] F. Wang, S. Williams, P. Colegrove, A. A. Antonysamy, Microstructure and mechanical properties of wire and arc additive manufactured Ti-6Al-4V, Metallurgical and Materials Transactions A 44 (2013) 968–977. https://doi.org/10.1007/s11661-012-1444-6

[5] X. Xiong, H. Zhang, G. Wang, Metal direct prototyping by using hybrid plasma deposition and milling, Journal of Materials Processing Technology 209 (2009) 124–130. https://doi.org/10.1016/j.jmatprotec.2008.01.059

[6] Q. Wu, J. Lu, C. Liu, X. Shi, Q. Ma, S. Tang, H. Fan, S. Ma, Obtaining uniform deposition with variable wire feeding direction during wire-feed additive manufacturing, Materials and Manufacturing Processes 32 (2017) 1881–1886. https://doi.org/10.1080/10426914.2017.1364860

[7] C. G. Pickin, S. W. Williams, M. Lunt, Characterisation of the cold metal transfer (CMT) process and its application for low dilution cladding, Journal of Materials Processing Technology 211 (2011) 496–502. https://doi.org/10.1016/j.jmatprotec.2010.11.005

[8] C. Pickin, K. Young, Evaluation of cold metal transfer (CMT) process for welding aluminium alloy, Science and Technology of Welding and Joining 11 (2006) 583–585. https://doi.org/10.1179/174329306X120886

[9] L. Troeger, E. Starke Jr., Microstructural and mechanical characterization of a superplastic 6xxx aluminum alloy, Materials Science and Engineering A 277 (2000) 102–113. https://doi.org/10.1016/S0921-5093(99)00543-2

[10] Y. Chi, N. Murali, J. Liu, M. Liese, X. Li, Wire arc additive manufacturing (WAAM) of nanotreated aluminum alloy 6061, Rapid Prototyping Journal 29 (2023) 1341–1349. https://doi.org/10.1108/RPJ-05-2022-0148

[11] B. Cong, J. Ding, S. Williams, Effect of arc mode in cold metal transfer process on porosity of additively manufactured Al-6.3%Cu alloy, The International Journal of Advanced Manufacturing Technology 76 (2015) 1593–1606. https://doi.org/10.1007/s00170-014-6346-x

[12] A. P. Boeira, I. L. Ferreira, A. Garcia, Alloy composition and metal/mold heat transfer efficiency affecting inverse segregation and porosity of as-cast Al-Cu alloys, Materials & Design 30 (2009) 2090–2098. https://doi.org/10.1016/j.matdes.2008.08.032

[13] M. Dinovitzer, X. Chen, J. Laliberte, X. Huang, H. Frei, Effect of wire and arc additive manufacturing (WAAM) process parameters on bead geometry and microstructure, Additive Manufacturing 26 (2019) 138–146. https://doi.org/10.1016/j.addma.2018.12.013

[14] Z. Qi, B. Cong, B. Qi, H. Sun, G. Zhao, J. Ding, Microstructure and mechanical properties of double-wire+arc additively manufactured Al-Cu-Mg alloys, Journal of Materials Processing Technology 255 (2018) 347–353. https://doi.org/10.1016/j.jmatprotec.2017.12.019

[15] Y. Baba, H. Yoshida, Intercrystalline embrittlement of age-hardened aluminum alloys and its prevention, Journal of Japan Institute of Light Metals 31 (1981) 195–205. https://doi.org/10.2464/jilm.31.195

[16] J. Xiong, G. Zhang, Z. Qiu, Y. Li, Vision-sensing and bead width control of a single-bead multi-layer part: Material and energy savings in GMAW-based rapid manufacturing, Journal of Cleaner Production 41 (2013) 82–88. https://doi.org/10.1016/j.jclepro.2012.10.009

[17] W. Zeli, Y. Zhang, A review of aluminum alloy fabricated by different processes of wire arc additive manufacturing, Materials Science 27 (2021) 18–26. https://doi.org/10.5755/j02.ms.22772

[18] Y. Luo, J. Li, J. Xu, L. Zhu, J. Han, C. Zhang, Influence of pulsed arc on the metal droplet deposited by projected transfer mode in wire-arc additive manufacturing, Journal of Materials Processing Technology 259 (2018) 353–360. https://doi.org/10.1016/j.jmatprotec.2018.04.047

[19] S. Suryakumar, K. Karunakaran, A. Bernard, U. Chandrasekhar, N. Raghavender, D. Sharma, Weld bead modeling and process optimization in hybrid layered manufacturing, Computer-Aided Design 43 (2011) 331–344. https://doi.org/10.1016/j.cad.2011.01.006

[20] Y. Zhang, Y. Chen, P. Li, A. T. Male, Weld deposition-based rapid prototyping: A preliminary study, Journal of Materials Processing Technology 135 (2003) 347–357. https://doi.org/10.1016/S0924-0136(02)00867-1

[21] J. Ding, P. Colegrove, J. Mehnen, S. Ganguly, P. S. Almeida, F. Wang, S. Williams, Thermo-mechanical analysis of wire and arc additive layer manufacturing process on large multi-layer parts, Computational Materials Science 50 (2011) 3315–3322. https://doi.org/10.1016/j.commatsci.2011.06.023

[22] J. Spencer, P. Dickens, C. Wykes, Rapid prototyping of metal parts by three-dimensional welding, Proceedings of the Institution of Mechanical Engineers, Part B: Journal of Engineering Manufacture 212 (1998) 175–182. https://doi.org/10.1243/0954405981515590

[23] M. Mughal, H. Fawad, R. Mufti, M. Siddique, Deformation modelling in layered manufacturing of metallic parts using gas metal arc welding: effect of process parameters, Modelling and Simulation in Materials Science and Engineering 13 (2005) 1187. https://doi.org/10.1088/0965-0393/13/7/013

[24] C. Qiu, N. J. Adkins, M. M. Attallah, Microstructure and tensile properties of selectively laser-melted and of HIPed laser-melted Ti-6Al-4V, Materials Science and Engineering A 578 (2013) 230–239. https://doi.org/10.1016/j.msea.2013.04.099

[25] A. Mertens, S. Reginster, H. Paydas, Q. Contrepois, T. Dormal, O. Lemaire, J. Lecomte-Beckers, Mechanical properties of alloy T-6Al-4V and of stainless steel 316L processed by selective laser melting: Influence of out-of-equilibrium microstructures, Powder Metallurgy 57 (2014) 184–189. https://doi.org/10.1179/1743290114Y.0000000092

[26] A. Khorasani, I. Gibson, U. S. Awan, A. Ghaderi, The effect of SLM process parameters on density, hardness, tensile strength and surface quality of Ti-6Al-4V, Additive Manufacturing 25 (2019) 176–186. https://doi.org/10.1016/j.addma.2018.09.002

[27] Y. Zhao, Y. Chen, Z. Wang, J. Ye, W. Zhao, Mechanical properties, microstructural characteristics and heat treatment effects of WAAM stainless-steel plate material, Journal of Building Engineering 75 (2023) 106988. https://doi.org/10.1016/j.jobe.2023.106988

[28] N. Lekkala, K. S. Prasad, Parametric optimization of weld bead of aluminium 6061 fabricated through wire arc additive manufacturing, Engineering Research Express 6 (2024) 046001. https://doi.org/10.1088/2631-8695/ad80fa

[29] V. T. Le, M. C. Bui, T. D. Nguyen, V. A. Nguyen, V. C. Nguyen, On the connection of the heat input to the forming quality in wire-and-arc additive manufacturing of stainless steels, Vacuum 209 (2023) 111807. https://doi.org/10.1016/j.vacuum.2023.111807

[30] H. Liu, H. Fujii, M. Maeda, K. Nogi, Tensile properties and fracture locations of friction-stir welded joints of 2017-T351 aluminum alloy, Journal of Materials Science Letters 22 (2003) 692–696. https://doi.org/10.1016/S0924-0136(03)00806-9